Cite this: DOI: 00.0000/xxxxxxxxxx

Signature of a conical intersection in the dissociative photoionization of formaldehyde†

Alexandre Zanchet,[a,b,c] Gustavo A. García,[d] Laurent Nahon,[d] Luis Bañares[a,e] and Sonia Marggi Poullain[a,f]

Received Date
Accepted Date

DOI: 00.0000/xxxxxxxxxx

The valence-shell photoionization of formaldehyde is investigated by means of combining Photo-Electron Photo-Ion in COincidence (PEPICO) experiments and *ab initio* calculations. The formation of three ion fragments: HCO^+, CO^+ and H_2^+, *via* dissociative photoionization following excitation at 17 eV is discussed. The experimental results consisting of electron-ion kinetic energy correlation diagrams for the corresponding coincident events, *i.e.* (HCO^+, e^-), (CO^+, e^-) and (H_2^+, e^-) as well as the fragment abundance as a function of the binding energy are complemented by high level electronic structure calculations including potential energy curves and on-the-fly trajectories. The results are consistent with a main relaxation process *via* internal conversion into rovibrationally excited levels of the H_2CO^+ ground state, followed by statistical dissociation, preferentially into HCO^+. The analysis of the experimental results reveals nevertheless the signature of a conical intersection controlling the dynamics and favoring dissociation into the molecular channel, $CO^+ + H_2$. In addition, the minor formation of the H_2^+ ion is suggested to occur through a roaming pathway on the cation excited state.

1 Introduction

Ionizing radiation plays a relevant role in a large number of areas from medicine, in particular for tumor destruction, to atmospheric sciences and astrochemistry. It widely contributes to the decay of pollutants in the troposphere producing radicals and ions while it is responsible of the formation of organic molecules in the interstellar medium (ISM). In this context, formaldehyde photoionization and photofragmentation is particularly interesting due to its role as a precursor of complex organic molecules in the ISM and of molecules of astrobiological interest[1–4]. In the present work, we investigate the valence-shell photoionization and subsequent dissociation of formaldehyde following VUV excitation in a joint experimental and theoretical study. Although the results presented are consistent with a main dissociation into the ionic ground state following relaxation *via* internal conversion, the direct signature of a conical intersection controlling the dissociative photoionization is also revealed and discussed.

In the past years, neutral formaldehyde photodissociation has received a lot of interest regarding, in particular, the roaming pathway[5–7]. This new mechanism bypasses completely the conventional saddle point transition state: the incipient hydrogen atom orbits the remaining part of the molecule until a reactive site is encountered and H_2 + CO are produced by intramolecular abstraction. In contrast, its photoionization and dissociative photoionization (DPI) has been less actively investigated[8–18]. From an experimental point of view, the ionization potentials and fragment appearance thresholds have been reported and different autoionizing n*s* and n*p* Rydberg series converging to the first and second excited states of H_2CO^+ have been identified[9]. Two main DPI channels were discussed based on the measured photoionization efficiency curves: the H-atom loss leading to HCO^+ + H, and the molecular channel, leading to CO^+ + H_2, characterized by a threshold appearance at 11.93 and 14.10 eV, respectively. The high-resolution photoelectron spectrum measured employing HeIα radiation was later reported and several vibrational progressions assigned to the $\widetilde{X}\ ^2B_2$, $\widetilde{A}\ ^2B_1$, $\widetilde{B}\ ^2A_1$ and $\widetilde{C}\ ^2B_2$ first electronic states of H_2CO^+, lying at 10.8, 14.10, 15.83, 16.23 eV, respectively, were resolved and analyzed.[15,16]

Theoretically, partial potential energy curves have been reported and discussed in terms of photofragmentation paths.[10,11,17,18] The CO^+ was suggested to be formed through a conical intersection found between the $\widetilde{B}\ ^2A_1$ and $\widetilde{A}\ ^2B_1$ states of H_2CO^+, while no curve crossing allowing the formation of HCO^+ was found, so that an internal conversion followed by slow dissociation on the ground state was proposed. Previous theoretical work is, however, rather limited and, in particular, it did not investigate the connection between the Franck-Condon region and the asymptotic region, *i.e.* at the dissociation limits. The picture on the dissociative photoionization of formaldehyde is therefore somewhat incomplete and many questions remain opened concerning the dynamics leading to the HCO^+, CO^+ and H_2^+, including the role of conical intersections and non-adiabatic dynamics.

The dissociative photoionization of formaldehyde is investigated here by means of photoion photoelectron coincidence (PEPICO) experiments following one-photon VUV excitation at 17 eV. The experimental results are complemented by high level *ab initio* calculations, including potential energy curves and on-the-fly trajectories. The electron-ion kinetic energy correlation diagrams recorded for the three main fragment ions, *i.e.*, HCO^+, CO^+ and H_2^+, reveal a major statistical dissociation process following vertical photoionization. The main relaxation process occurs through internal conversion into rovibrationally excited levels of the H_2CO^+ ground state, followed by its fragmentation, preferentially into HCO^+. The results highlight, nevertheless, the signature of a conical intersection opening an efficient and prompt pathway for the CO^+ formation in the Franck-Condon gap.

[0a] *Departamento de Química Física (Unidad Asociada de I+D+i al CSIC), Facultad de Ciencias Químicas, Universidad Complutense de Madrid, 28040 Madrid, Spain; E-mail: smarggi@ucm.es*
[0b] *Instituto de Física Fundamental, Consejo Superior de Investigaciones Científicas, C/ Serrano, 123, 28006 Madrid, Spain*
[0c] *Departamento de Química Física, Facultad de Ciencias Químicas, Universidad de Salamanca,37008 Salamanca, Spain*
[0d] *Synchrotron SOLEIL, L'Orme des Merisiers, St. Aubin, BP 48, 91192 Gif sur Yvette, France*
[0e] *Instituto Madrileño de Estudios Avanzados en Nanociencia (IMDEA-Nanoscience), Cantoblanco, 28049 Madrid, Spain*
[0f] *Department of Chemistry, University of California, Berkeley, CA94720, USA*

[0†] Electronic Supplementary Information (ESI) available: Time-of-flight mass spectra following ionization at $h\nu$ = 17 eV and 18.5 eV and results (including all relevant KECDs) following dissociative photoionization at $h\nu$ = 18.5 eV. Theoretical information: active orbitals and geometries. See DOI: 00.0000/00000000.

The experimental set-up and the theoretical methodology are summarized in the next section while in Section 3 the experimental and theoretical results are presented and discussed. Finally, some conclusions are presented in Section 4.

2 Methods

2.1 Experimental Set-up

Experiments were performed at the DESIRS beamline of the French synchrotron SOLEIL,[19] on the permanent end-station SAPHIRS,[20] employing the PEPICO spectrometer DELICIOUS III[21]. Synchrotron photons emitted from an undulator were dispersed by a 6.65 m normal incidence monochromator. A 200 l mm^{-1} grating was chosen and the monochromator slits were set to provide a photon energy resolution of $\sim$ 3 meV. The absolute photon energy scale was calibrated separately within an accuracy of 1 meV using the absorption lines of Ar in the gas filter. Pure paraformaldehyde (Sigma Aldrich) was placed on an oven heated at 70 °C to produce formaldehyde and water. A filter containing $MgSO_4$ was employed to eliminate the water. The resulting formaldehyde was expanded through a 50 mm diameter nozzle and collimated by a skimmer (Beam Dynamics, 1.0 mm diameter) to form a continuous molecular beam.

The molecular beam crossed the synchrotron light at a right angle in the center of DELICIOUS III, and all electrons and ions produced were extracted and accelerated in opposite directions by an electric field. Velocity map imaging (VMI) and a modified Wiley-McLaren time-of-flight (TOF) imaging spectrometers were employed to detect electrons and ions, respectively. Photoelectron energy spectra (PES) and angular distributions were obtained from the electron VMI image via an Abel inversion algorithm while the full ion 3D momentum distribution was extracted from the ion TOF and the 2D arrival position onto the corresponding position-sensitive detector (PSD). The coincidence scheme yielded electron images, and thus PES correlated to a particular mass and ion momentum, which in turn produced the electron and ion kinetic energy correlation diagram.

The errors bars shown in Fig. 2 have been obtained assuming a Poisson distribution on the mass-selected photoelectron images, which is then carried through the Abel inversion operations using standard error propagation formulas.

2.2 Theory

High level electronic structure calculations were carried out at the internally contracted multireference configuration interaction (MRCI) level employing the MOLPRO package[22] and the aug-cc-pVTZ basis set. The active space selected includes the $2s$ and $2p$ orbitals of C and O atoms and the $1s$ orbitals of both H atoms, leading to 10 active orbitals (See ESI and Fig. S4†) while the $1s$ orbitals of carbon and oxygen were kept frozen. The calculations, performed in C_s symmetry, include the state averaging of 4 states of A' symmetry and 3 states of A'' symmetry of H_2CO^+ along with the ground state $1A'$ and $1A''$ of neutral H_2CO. For the electronic states of the cation, 11 electrons are included in the active space while 12 for the two states of the neutral formaldehyde. Potential energy curves have been computed for both the H-atom loss and the $(CO+H_2)^+$ channels. Since the Davidson correction does not affect in the same way all the electronic states, accounting for it may lead to fictive crossings between the adiabatic curves, and therefore, the curves presented have been obtained at a pure MRCI level. A thorough search of stationary points on the potential energy surfaces have also been carried out at the same level. Finally, on-the-fly trajectory calculations have been performed on the ground state potential energy surface employing the miQCT code[23–26] coupled to MOLPRO. In order to obtain an analytic gradient and a more affordable cpu time, these calculations were performed employing Complete Active Space with Second-order Perturbation Theory (CASPT2) instead of MRCI.

3 Results and Discussion

Following excitation at 17 eV, three ion fragments from dissociative photoionization (DPI) are produced: HCO^+, CO^+ and H_2^+, as observed in the time-of-flight ion mass spectrum (see ESI†). $HCO^+ + e^-$ following H-atom loss is the main channel characterized by a branching ratio of 71%, while the formation of $CO^+ + H_2$ represents around 27% of the total DPI signal. Finally, a minor formation of $H_2^+ + CO$ is observed, with a branching ratio around 1%. Complementary measurements were carried out at the higher excitation energy of 18.5 eV. The results obtained (see ESI†) are consistent with the results presented here at 17 eV, reflecting a similar photoionization and subsequent dissociation dynamics. A minor formation of H^+, representing 0.1%, was nevertheless observed in agreement with the experimental threshold for the $HCO + H^+$ channel reported at 17.41 eV.[8,13] The electron-ion kinetic energy correlation diagrams (KECD), *i.e.* the number of events as a function of the ion kinetic energy release (KER) and the photoelectron energy (E_e), for the three DPI channels, (HCO^+, e^-), (CO^+, e^-) and (H_2^+, e^-) coincident events following excitation at 17 eV are presented in Figure 1 along with the corresponding photoelectron spectra, which are compared to the HeIα photoelectron spectrum reported by Carlsson-Göthe and Karlsson.[15]

As observed in Fig. 1 (left panel, see inset), the H-atom loss channel is characterized by an ion translational energy Boltzmann-type distribution. A series of structures are resolved in the photoelectron energy spectrum (PES) and assigned to the initial photoionization into different vibrational levels of the $\widetilde{A}\,^2B_1$ and $\widetilde{B}\,^2A_1$ electronic excited states. Although some differences in the relative intensities are observed, the PES measured here appears in good agreement with the reported HeIα PES. The HCO^+ channel is therefore produced through a first vertical photoionization. The vertical lines observed in the KECD (Fig. 1) reflect a sequential process characterized by a slow H-atom loss, following ionization. A prompt DPI process through repulsive ionic electronic states is often characterized by diagonal lines along the available energy in the KECD, reflecting the sharing between the electron energy and the ion-fragment translational energy. In the present case, the available energy after vertical photoionization is strongly transferred into internal motion, in spite of the KER of the fragment, giving rise to the Boltzmann-type ion energy distribution. This is typical of a unimolecular statistical dissociation process, in agreement with previous investigations suggesting fragmentation *via* internal conversion and slow dissociation in the ground state leading to HCO^+.

Similarly, the (CO^+, e^-) DPI channel is characterized in Fig. 1 (central panel) by a Boltzmann-type KER distribution and a series of resolved peaks in the PES assigned to the vertical photoionization into $H_2CO^+(\widetilde{B}\,^2A_1, \nu)$. In contrast to the H-atom loss channel, photoionization into $H_2CO^+(\widetilde{A}\,^2B_1)$ for binding energies below 15 eV does not seem to lead to CO^+ formation. Some structures can

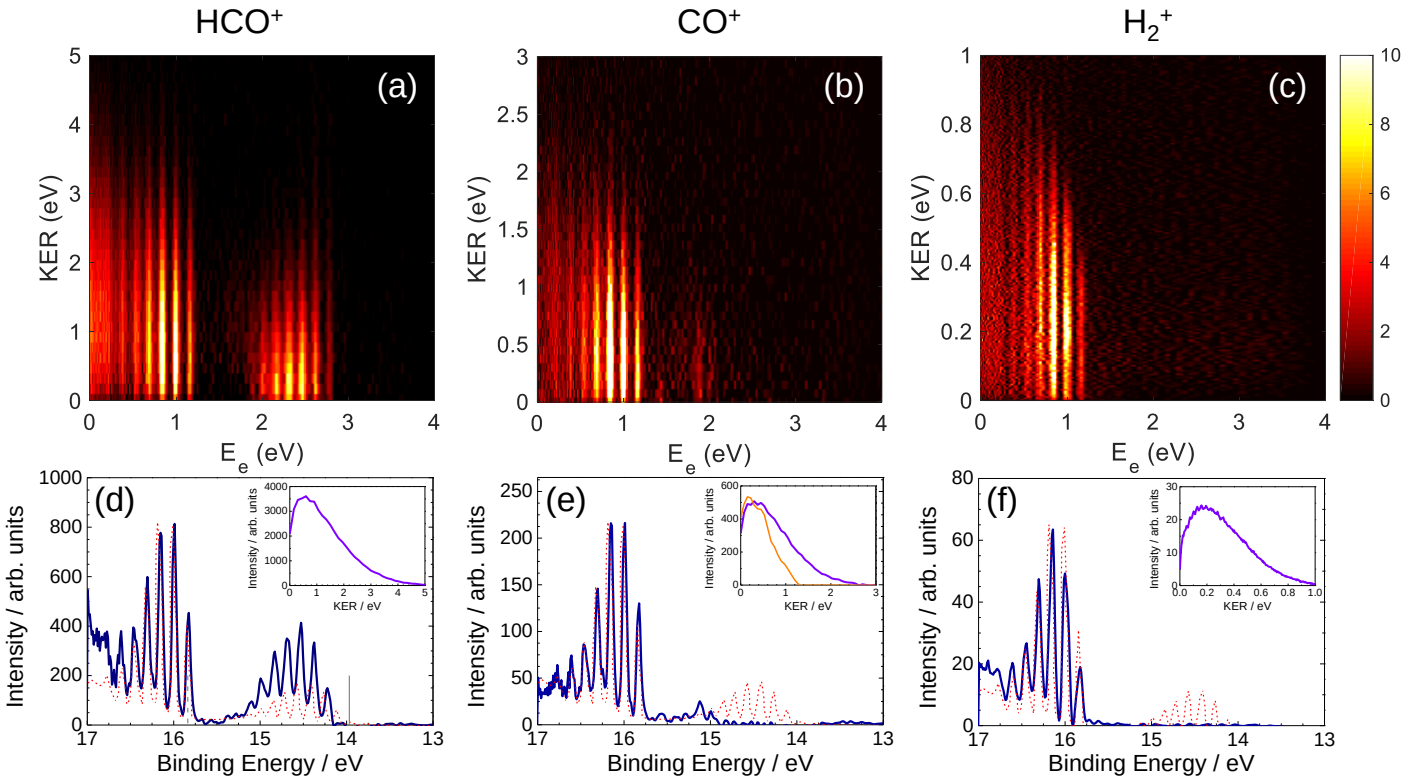

Figure 1 Electron-ion kinetic energy correlation diagram, KER *vs.* E_e, for (HCO^+, e^-) (a), (CO^+, e^-) (b) and (H_2^+, e^-) (c) coincident events following excitation at 17 eV. The colorbar shows the scale for (b) and must be x5 for (a) and x0.1 for (c). The corresponding photoelectron spectrum (blue line) compared to the reported HeIα PES[15] (red dashed line) are shown in (d)-(f). The corresponding ion translational energy distributions for all E_e are represented in the inset. In (e), the distribution obtained for E_e = 1.3-2.2 eV (E_{bind} = 15.2-15.7 eV) is represented by an orange line. Vertical grey bars in (d) represent the binding energy for H_2CO^+ $\widetilde{A}\,^2B_1$ (solid line) and $\widetilde{B}\,^2A_1$ (dashed line) ionic electronic states in their ground vibrational state, from Ref.[15].

be discerned, however, between 15 and 15.8 eV, which are barely perceptible in the HeIα PES (dashed red line). These interesting contributions highlight some non Franck-Condon photoionization into high vibrational levels of the $\widetilde{A}\,^2B_1$ state. In contrast to the KER distribution extending up to 2 eV after photoionization into the $H_2CO^+\widetilde{B}$ state, a narrower Gaussian peak at threshold energies, characterized by a full width at half maximum around 1 eV, is observed for the structures around 15.6 eV (E_e=1.4 eV).

Finally, a similar KECD is recovered for the second molecular channel, (H_2^+, e^-) as observed in Fig. 1 (right panel). H_2^+ is formed following vertical photoionization into $H_2CO^+(\widetilde{B}\,^2A_1, v)$ state and characterized by a Boltzmann-type ion energy distribution. According to Fig. 1, the three DPI channels seem to be characterized by statistical dissociation processes and may reflect a prior relaxation into the H_2CO^+ ground state following vertical photoionization.

One great advantage of the PEPICO technique is the possibility to extract the fragment branching ratio as a function of the binding energy, E_{bind}. Such fragment abundance diagram is depicted in Figure 2. At energies lower than 15 eV, nearly 100% of the formaldehyde photofragmentation proceeds through a H-atom elimination DPI channel, although the CO^+ appearance threshold was reported at 14.1 eV.[9] At approximately 14.9 eV, the H_2 elimination channel seems to open more efficiently leading to a growing abundance of CO^+ produced up to approximately 20%. On the other hand, the H_2^+ formation opens at ≈15.5 eV, but remains a minor channel. A striking broad resonance is observed between 15.4 and 15.8 eV, peaking at 15.6 eV. The relative abundance of HCO^+ drops significantly while that of CO^+ increase, both of them becoming nearly equal. This interesting feature reflects a pathway leading to a very effective fragmentation into CO^+ at that binding energy.

The potential energy curves leading to the H-atom loss channels, *i.e.* $(H + HCO)^+$, and to the molecular channels $(H_2 + CO)^+$ have been computed and are depicted in Figure 3. The corresponding vertical excitation energies for the different ionic states from the present calculations are summarized in Table 1 along with the experimental values[15,16], showing an excellent agreement. The correspondence between the electronic states in C_{2v} symmetry and the ones computed here in C_s symmetry is specified in Table 1 while the electronic transition leading to each excited state is detailed in the ESI†. We remark that in the present work we employ the coordinate system chosen by Bruna *et al.*[18]. A different coordinate system was used in the early calculations from Domcke and Cederbaum,[10] where the planes of symmetry were inverted resulting therefore in an inversion of B_1 and B_2 symmetries of the computed electronic states. The fourth H_2CO^+ electronic state named $\widetilde{C}^2B_1$, is then equivalent to the $\widetilde{C}^2B_2$ label in previous experimental photoelectron spectra.[13,15,16] A fifth electronic state, $\widetilde{D}\,^2B_2$, not reported experimentally, also resulted from the calculations in agreement with Ref.[18].

The curves leading to $(HCO + H)^+$ have been obtained by stretching one of the C-H bonds, the HCO remaining frozen, while the curves into $(CO + H_2)^+$ have been calculated by stretching the distance between the C atom and the center-of-mass of H_2 and relaxing

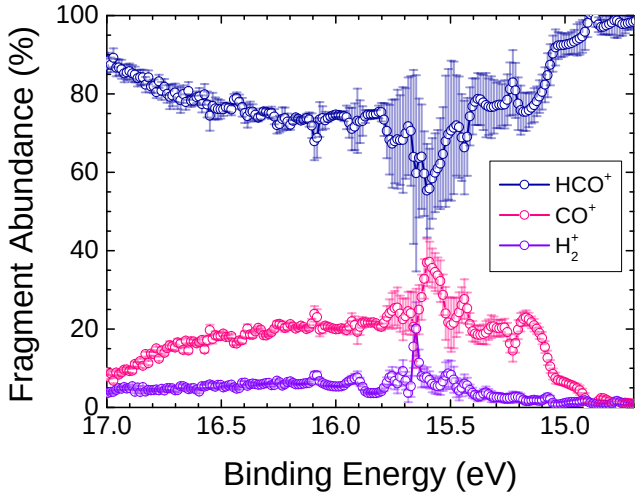

Figure 2 Fragment abundance (in %) as a function of the binding energy (E_{bind}).

Table 1 Theoretical and experimental adiabatic ionization energies (eV).

H_2CO^+ states	C_s symmetry	Exp.[16]	Exp.[15]	This work (Theory)
$\widetilde{X}\,^2B_2$	$^2A'$	10.8887	10.885	10.83
$\widetilde{A}\,^2B_1$	$^2A''$	14.1024	13.968	14.10
$\widetilde{B}\,^2A_1$	$^2A'$	15.8375	15.837	15.75
$\widetilde{C}\,^2B_1$	$^2A''$	16.2395	16.241	16.31
$\widetilde{D}\,^2B_2$	$^2A'$	–	–	16.88

the system in the cation ground state. For the H-atom loss channel, all electronic states present a bound shape as a function of R_{C-H}, as observed in Fig. 3(a). No prompt direct dissociation pathway leading to H-atom loss seems opened following ionization in this excitation energy range. In contrast, a conical intersection between the $\widetilde{X}\,^2B_2$ and $\widetilde{B}\,^2A_1$ ionic states, *i.e.* $\widetilde{X}\,^2A'$ and $\widetilde{B}\,^2A'$ in C_s symmetry, located at 15.6 eV is found to control the dissociation into the molecular channel. It is a typical case of symmetry-induced conical intersection: both states can cross in C_{2v} symmetry, while they repel each other as soon as the C_{2v} symmetry is broken since they both correlate to A' states in C_s.

Since the PECs are built by relaxing the cation ground state, the asymptotic values of the excited states in the curves are only indicative. In order to obtain the correct dissociation energies for the different channels, an additional geometry optimization of the different fragments in their excited states was also performed, and the results are presented in Table 2. The appearance energies (AE) for the parent and all fragment ions measured by Guyon *et al.*[9] and Bombach *et al.*[13] are also specified and compared to the present experiments. A very good agreement is obtained between the first theoretical dissociation limits and the ion appearance thresholds for HCO^+ and CO^+ ions from Guyon *et al.*[9], located at 11.9 and 14.1 eV, respectively. No barrier seems then to control the probability for dissociative photoionization into HCO^+ and CO^+. In the present experiments, no CO^+ is observed following ionization into the $\widetilde{A}\,^2B_1$ state below E_{bind}=14.9 eV in agreement with the reported AE from Ref.[13], although some CO^+ could be present in the background on Fig. 1(b). A significant increase in the CO^+ production for $h\nu \geqslant$ 14.8-15 eV is indeed observed in Guyon *et al.* work[9]. Taking into account the remarkable change in the H-H internuclear distance associated to this channel, the efficient CO^+ production for binding energies $E_{bind} \geqslant$ 14.9 eV may reflect a more favorable dissociation through formation of the H_2 co-fragment vibrationally excited. The formation of CO^+ below E_{bind} = 14.9 eV, could be attributed to the dissociation of superexcited states (most likely, Rydberg states) into H_2 + CO, followed by autoionization of the excited CO, as previously suggested[9].

Additionally, the H-atom loss channel leading to HCO^+ is predicted to open at energies around 12.1 eV, while at lower energies photoionization of formaldehyde will exclusively lead to H_2CO^+. In contrast, the dissociation energy to produce HCO^+ and CO^+ in their first excited electronic state is higher, 17.94 eV and 16.5 eV, respectively. Therefore, all the CO^+ and HCO^+ ions detected following vertical photoionization into binding energies E_{bind} below these values have to be produced after relaxation to the H_2CO^+ ground state. Since the excitation energy is selected at 17 eV, only a small part of the CO^+ is produced after photoionization at $E_{bind} \geq$ 16.5 eV and could then be due to slow dissociation in the upper electronic states. Several crossings characterize this region in the PECs (Fig. 3(b)) so that the dissociation mechanism appears rather entangled. Taking into account the KECD in Fig. 1, this reaction pathway is nevertheless rather minor.

Otherwise, the branching ratio between HCO^+ and CO^+ will be determined by the relaxation mechanism and the further dynamics on the ground state. Taking into account the PECs depicted in Fig. 3, two reaction pathways are possible for relaxation: either through

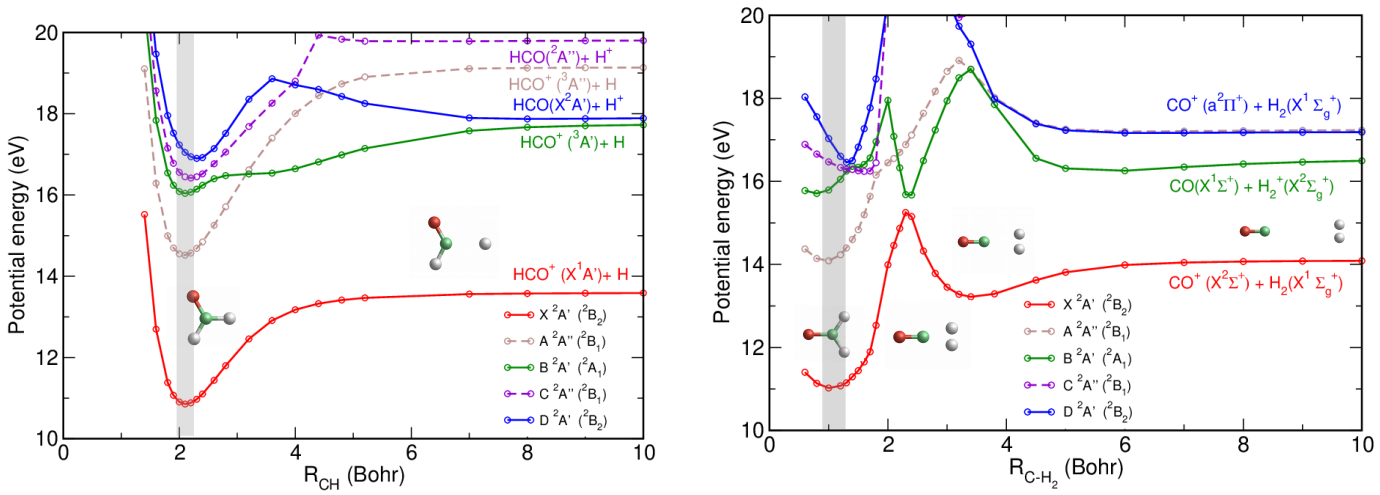

Figure 3 Potential energy curves of H_2CO^+ (in C_s symmetry) leading to $(HCO+H)^+$ (top) and to $(H_2+CO)^+$ (bottom) as a function of R_{C-H} and R_{C-H_2}, respectively. Energies are referred to the ground state of the neutral formaldehyde in its equilibrium position. The grey area illustrates the Franck-Condon region associated to the vertical one-photon ionization from the neutral ground state.

Table 2 Theoretical dissociation limits (D_e) of the different products referred to the neutral species and the ground state of the cation. The experimental appearance energies for the different ionic fragments obtained from the present experiments and from Ref.[9] and Ref.[13] are also indicated.

Fragment species	D_e [H_2CO]	D_e [H_2CO^+]	Exp.	Appearance	Energies
			Ref.[9]	Ref.[13]	Present work
H_2CO^+	10.85	0	10.868	–	–
$H(^2S)$ + $HCO^+(\widetilde{X}\ ^1\Sigma^+)$	12.14	1.29	11.926	14.10	14.1
$H_2(X\ ^1\Sigma^+)$ + $CO^+(X\ ^2\Sigma^+)$	14.09	3.24	14.10	14.82	14.9
$H(^2S)$ + $COH^+(X\ ^1A')$	14.22	3.37	–	–	–
$H_2^+(X\ ^2\Sigma^+)$ + $CO(X\ ^1\Sigma^+)$	15.48	4.63	–	15.85	15.5
$H_2(X\ ^1\Sigma^+)$ + $CO^+(1\ ^2\Pi)$	16.50	5.65	–	–	–
H^+ + $HCO(\widetilde{X}\ ^2A')$	17.70	6.85	–	17.50	17.32
$H(^2S)$ + $HCO^+(1\ ^3A')$	17.94	7.09	–	–	
H^+ + $HCO(1\ ^2\Pi)$	18.76	7.91	–	–	
$H(^2S)$ + $HCO^+(1\ ^3A'')$	18.79	7.94	–	–	
$H(^2S)$ + $HCO^+(1\ ^1A'')$	19.41	8.56	–	–	
$H(^2S)$ + $HCO^+(2\ ^3A')$	19.85	9.00	–	–	

internal conversion to highly rovibrationally excited levels of $H_2CO^+(\widetilde{X})$ or mediated by the conical intersection observed in Fig. 3(b). This second relaxation mechanism was already suggested though in Ref.[17] as the probable pathway to form CO^+.

Since each vibrational mode can be employed as an orthogonal basis describing the position of the atoms, the coordinates used for the curves computed here can be *projected* into the normal mode coordinates. Two stretching vibrational modes are of relevance here: the CH_2 symmetric stretch and the CH_2 asymmetric stretch. A maximum overlap is indeed found between the normal coordinates of this last mode and the Jacobi coordinates employed in the H-atom loss curves, while the coordinates used for the $(H_2 + CO)^+$ curves can be projected into the ones of the CH_2 symmetric stretch with a great overlap. The curves leading to HCO^+ depicted in Fig. 3(a) are therefore directly related to the CH_2 asymmetric stretching vibrational mode, while the curves for the molecular channel in Fig. 3(b) are related to the CH_2 symmetric stretching mode. Relaxation through internal conversion can occur through the CH_2 symmetric stretch, but not along the CH_2 asymmetric stretching mode. Due to energy conservation, internal conversion can only occur between bound ro-vibrational levels of different electronic states lying at a comparable energy. As observed in Fig. 3(a), no bound ro-vibrational levels of the ground state overlap with the $\widetilde{A}\ ^2B_1$ first electronic state. On the contrary, this overlap between bound ro-vibrational states is pretty favorable in Fig. 3(b) and the internal conversion can then take place through the CH_2 symmetric stretch.

In order to deepen our understanding of the dissociation on the H_2CO^+ ground state following relaxation, further calculations have been performed including an extensive study of stationary points on the potential energy surface and *on-the-fly* classical trajectories. Taking into account the KECDs measured experimentally (Fig. 1), statistical dissociation would occur following relaxation into the ground state. A total of 100 on-the-fly trajectories were launched at CASPT2 level using the miQCT code[23–26] coupled to MOLPRO. The initial conditions were determined by running *normal mode* trajectories for several highly excited rovibrational levels lying at energies of ≈3.65 eV, ≈4.1 eV, ≈5.2 eV and ≈6.4 eV above the ionic rovibrational ground state. Only 2 out of 100 trajectories were found to finish producing CO^+, and both were obtained for the higher rovibrational level considered. The rest of the trajectories ended up

dissociating into HCO^+ regardless of the initial rovibrational state populated after relaxation.

A diagram summarizing the stationary points found on the potential energy surface of the H_2CO^+ ground state is displayed in Figure 4. The HCO^+ channel is characterized by the lower transition state; a dominant formation is therefore expected in agreement with the results from the on-the-fly trajectories. In contrast, the CO^+ channel lies at relatively higher energy and requires an additional migration of both H atoms. The dissociation dynamics following relaxation into the $H_2CO^+(X)$ through internal conversion would start in the region of the global minimum with a great excess of energy. The HCO^+ channel is therefore directly accessible from the minimum since no barriers to the dissociation energy need to be overcome. The CO^+ formation is, in contrast, rather unfavorable since it implies either to overcome, *via* a direct pathway, a much higher barrier ($> 4eV$) corresponding to the conical intersection, or to survive for a long time through an indirect dissociation. Both are highly unlikely taking into account the favorable formation of HCO^+. On the contrary, relaxation from the ro-vibrationally excited H_2CO^+ ($\widetilde{A}\,^2B_1$) through the conical intersection, as observed in Fig. 3(b), would lead the system into the *good* side of the barrier, allowing to directly dissociate into $CO^+ + H_2$. While the overall ratio of $\sim 25\%$ of CO^+ measured in the present experiments can reflect the contribution of all these mechanisms, this last dissociation pathway explains the peak at $\sim$50% observed for binding energies of 15.6 eV (see Fig. 2), matching the calculated position of the conical intersection (See Fig. 3 (bottom)). Such relaxation through the conical intersection would not favor the H-atom loss channel, since it would require overcoming the barrier.

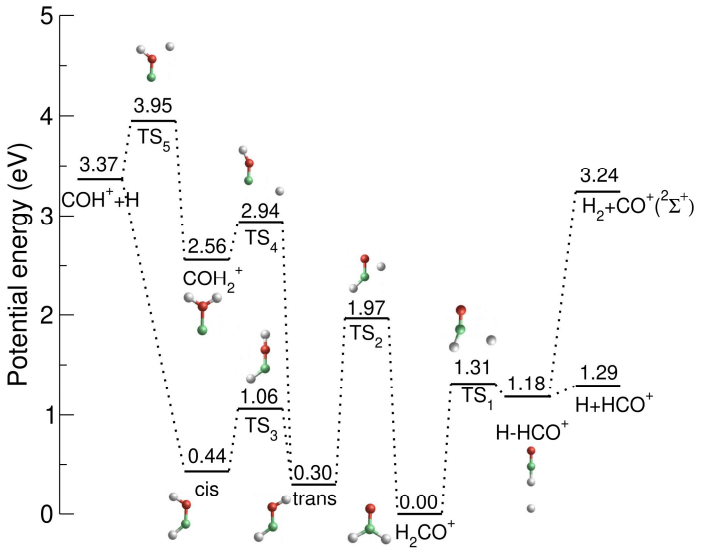

Figure 4 Stationary points of the potential energy surface of the ground state of H_2CO^+. Relevant geometries are also depicted while all geometries are shown in Fig. S5†.

Stationary points have also been searched on the excited states. Regarding the H^+ channel, no additional barrier than the endothermicity has been found on the second excited state, so that it is natural that the H^+ channel opens experimentally at the threshold. In addition, the search for stationary points also revealed a high barrier for the formation of H_2^+, occurring at higher energies. Taking into account that, experimentally H_2^+ is formed following photoionization into binding energies close to its appearance threshold, a roaming mechanism on the excited state is presumably involved in order to bypass the saddle point. Nevertheless, the mechanism leading to H_2^+ could not be unraveled in the present investigation despite all the computational efforts.

The remarkable resonance peaking around 15.6 eV observed in Fig. 2 reflects a more favorable formation of CO^+ at this binding energy and, therefore, a major role of the conical intersection, which has been calculated at this approximate energy, as observed in Fig. 3(b). Vertical photoionization into the highly vibrational levels of $H_2CO^+(\widetilde{A}\,^2B_1)$ at this binding energy is rather unfavorable considering the low Franck-Condon factors, as reflected in the reported HeIα PES in Fig. 1. A small structure is nevertheless observed between 15 and 16 eV in the PES, specially in the one associated to the formation of CO^+. The conical intersection controls the dynamics before and after: photoionization at these binding energies constitutes a favorable pathway for CO^+ formation. This structure is observed with less intensity in the PES corresponding to the H-atom loss channel, which confirms therefore that the relaxation through the conical intersection would lead preferentially to the molecular channel. The Gaussian-type KER distribution centered at threshold energies (see inset Fig. 1(e), orange line) characterizing this reaction pathway reflects a rather fast dissociation producing H_2 vibrationally excited. Such vibrational activity is likely acquired during dissociation taking into account the remarkable change in the H-H distance. Although a large amount of the available energy is transferred into this vibrational excitation and therefore, the translational energy is low, this direct dissociation pathway does not allow any redistribution, leading to the observed Gaussian peak. In a slow process, the available energy can be easily redistributed into other degrees of freedom leading to a Boltzmann-type distribution as observed in Fig. 1(e) (violet line) for CO^+ following photoionization into $H_2CO^+\widetilde{B}$ state, in contrast with the prompt dissociation mechanism through the conical intersection. Despite the low probability to photoionize into these ro-vibrational levels between 15 and 16 eV, the conical intersection opens an effective relaxation pathway and a very fast fragmentation mechanism. The small structure in the PES for (CO^+, e^-) along with the corresponding resonance in Fig. 2 is a direct signature of the conical intersection.

4 Conclusions

In conclusion, we report here a joint experimental and theoretical investigation on the valence-shell photoionization of formaldehyde, focusing on the formation of three ion fragments: HCO^+, CO^+ and H_2^+. The experimental results consisting of electron-ion kinetic energy correlation diagrams for the corresponding coincident events, *i.e.* (HCO^+, e^-), (CO^+, e^-) and (H_2^+, e^-), as well as the fragment abundance as a function of the binding energy, are complemented by high level electronic structure calculations including potential energy curves and on-the-fly trajectories. The results are consistent with a major relaxation *via* internal conversion into ro-vibrationally excited levels of the H_2CO^+ ground state, followed by its statistical fragmentation. The potential energy curves suggest that the relaxation is mediated by the CH symmetric stretch mode while in a second step, the distortion provided by the asymmetric stretch motion of the two CH combined with the excess of energy in other modes, and in particular the symmetric stretch mode, favors the expulsion of one of the hydrogens, leading preferentially to HCO^+. The analysis of the experimental results reveals nevertheless the signature of a conical intersection controlling the dissociation at long C-H_2 distances, in the Franck-Condon gap, and favoring the formation of the molecular channel, $CO^+ + H_2$. In addition, the minor formation of the H_2^+ ion is suggested to occur through a roaming pathway on the cation excited state since H_2^+ is formed following photoionization into binding energies close to its appearance threshold while a high barrier characterizes this channel in the calculations. Future time-resolved experiments will be particularly interesting. The role of the conical intersection in the CO^+ formation would likely appears in a short time-scale ($\leq$ 100 fs) while long time-scale dynamics (up to few picoseconds) would characterize the roaming pathway leading to the H_2^+ elimination.

Conflicts of interest

There are no conflicts to declare.

Acknowledgements

We thank Garikoitz Balerdi for his help in the first stages of this project. This work was performed at the DESIRS beamline. We acknowledge SOLEIL for provision of synchrotron radiation facilities under proposal number 20141243, and J.-F. Gil for his technical assistance. This project has received funding from the European Union's Horizon 2020 research and innovation programme under the Marie Sklodowska-Curie grant agreement No 842539 (ATTO-CONTROL) and has been financed in part by the Spanish MINECO (grant CTQ2015-65033-P) and the Spanish Ministry of Science and Innovation (grant PGC2018-096444-B-I00).

Notes and references

[1] D. Halfen, A. Apponi, N. Woolf, R. Polt and L. M. Ziurys, *The Astrophysical Journal*, 2006, **639**, 237.

[2] S. K. Blair, L. Magnani, J. Brand and J. G. Wouterloot, *Astrobiology*, 2008, **8**, 59–73.

[3] V. Guzmán, J. Pety, J. Goicoechea, M. Gerin and E. Roueff, *Astronomy & Astrophysics*, 2011, **534**, A49.

[4] A. Ocaña, E. Jiménez, B. Ballesteros, A. Canosa, M. Antiñolo, J. Albaladejo, M. Agúndez, J. Cernicharo, A. Zanchet, P. Del Mazo *et al.*, *The Astrophysical Journal*, 2017, **850**, 28.

[5] D. Townsend, S. A. Lahankar, S. K. Lee, S. D. Chambreau, A. G. Suits, X. Zhang, J. Rheinecker, L. Harding and J. M. Bowman, *Science*, 2004, **306**, 1158–1161.

[6] N. Herath and A. G. Suits, *The Journal of Physical Chemistry Letters*, 2011, **2**, 642–647.

[7] B. C. Shepler, Y. Han and J. M. Bowman, *The Journal of Physical Chemistry Letters*, 2011, **2**, 834–838.

[8] P. Warneck, *Zeitschrift für Naturforschung A*, 1971, **26**, 2047–2057.

[9] P. M. Guyon, W. A. Chupka and J. Berkowitz, *The Journal of Chemical Physics*, 1976, **64**, 1419–1436.

[10] W. Domcke and L. Cederbaum, *The Journal of Chemical Physics*, 1976, **64**, 612–625.

[11] M. V. Pires, C. Galloy and J. C. Lorquet, *The Journal of Chemical Physics*, 1978, **69**, 3242–3249.

[12] R. Bombach, J. Dannacher, J.-P. Stadelmann and J. Vogt, *Chemical Physics Letters*, 1980, **76**, 429–432.

[13] R. Bombach, J. Dannacher, J.-P. Stadelmann and J. Vogt, *International Journal of Mass Spectrometry and Ion Physics*, 1981, **40**, 275–285.

[14] P. C. Burgers, A. A. Mommers and J. Holmes, *Journal of the American Chemical Society*, 1983, **105**, 5976–5979.

[15] M. C. Göthe and L. Karlsson, *A High Resolution HeI Excited Photoelectron Spectrum of the H2CO Molecule*, Uppsala university, sweden technical report, 1990.

[16] B. Niu, D. A. Shirley and Y. Bai, *The Journal of chemical physics*, 1993, **98**, 4377–4390.

[17] C. Barbier, C. Galloy and J.-C. Lorquet, *The Journal of chemical physics*, 1984, **81**, 2975–2980.

[18] P. J. Bruna, M. R. J. Hachey and F. Grein, *Molecular Physics*, 1998, **94**, 917–928.

[19] L. Nahon, N. de Oliveira, G. A. Garcia, J.-F. Gil, B. Pilette, O. Marcouillé, B. Lagarde and F. Polack, *Journal of Synchrotron Radiation*, 2012, **19**, 508–520.

[20] X. Tang, G. A. Garcia, J.-F. Gil and L. Nahon, *Review of Scientific Instruments*, 2015, **86**, 123108.

[21] G. Garcia, B. Cunha de Miranda, M. Tia, S. Daly and L. Nahon, *Review of Scientific Instruments*, 2013, **84**, 053112.

[22] H.-J. Werner, P. J. Knowles, G. Knizia, F. R. Manby, M. Schütz, P. Celani, T. Korona, R. Lindh, A. Mitrushenkov, G. Rauhut, K. R. Shamasundar, T. B. Adler, R. D. Amos, A. Bernhardsson, A. Berning, D. L. Cooper, M. J. O. Deegan, A. J. Dobbyn, F. Eckert, E. Goll, C. Hampel, A. Hesselmann, G. Hetzer, T. Hrenar, G. Jansen, C. Köppl, Y. Liu, A. W. Lloyd, R. A. Mata, A. J. May, S. J. McNicholas, W. Meyer, M. E. Mura, A. Nicklass, D. P. O'Neill, P. Palmieri, D. Peng, K. Pflüger, R. Pitzer, M. Reiher, T. Shiozaki, H. Stoll, A. J. Stone, R. Tarroni, T. Thorsteinsson and M. Wang, *MOLPRO, version 2015.1, a package of ab initio programs*, 2015, see.

[23] A. Dorta-Urra, A. Zanchet, O. Roncero and A. Aguado, *The Journal of Chemical Physics*, 2015, **142**, 154301.

[24] A. Zanchet, O. Roncero and N. Bulut, *Physical Chemistry Chemical Physics*, 2016, **18**, 11391–11400.

[25] A. Zanchet, P. del Mazo, A. Aguado, O. Roncero, E. Jiménez, A. Canosa, M. Agúndez and J. Cernicharo, *Physical Chemistry Chemical Physics*, 2018, **20**, 5415–5426.

[26] O. Roncero, A. Zanchet and A. Aguado, *Physical Chemistry Chemical Physics*, 2018, **20**, 25951–25958.